Rapid Communications | Editors' Suggestion

Observation of interface superconductivity in a $SnSe_2$/epitaxial graphene van der Waals heterostructure

Yi-Min Zhang,[1] Jia-Qi Fan,[1] Wen-Lin Wang,[1] Ding Zhang,[1,2] Lili Wang,[1,2] Wei Li,[1,2] Ke He,[1,2] Can-Li Song,[1,2,*] Xu-Cun Ma,[1,2,†] and Qi-Kun Xue[1,2,‡]

[1]*State Key Laboratory of Low-Dimensional Quantum Physics, Department of Physics, Tsinghua University, Beijing 100084, China*

[2]*Collaborative Innovation Center of Quantum Matter, Beijing 100084, China*

(Received 28 February 2018; revised manuscript received 30 November 2018; published 19 December 2018)

We report on direct observation of interface superconductivity in single-unit-cell $SnSe_2$ films grown on graphitized SiC(0001) substrate. The tunneling spectrum in the superconducting state reveals a rather conventional character with a fully gapped order parameter. The occurrence of superconductivity is further confirmed by the observation of vortices under external magnetic field. Through interface engineering, we unravel the mechanism of superconductivity that originates from a two-dimensional electron gas formed at the interface of $SnSe_2$ and graphene. Our finding opens up novel strategies to hunt for and understand interface superconductivity based on van der Waals heterostructures.

DOI: 10.1103/PhysRevB.98.220508

Interface superconductivity has recently been the subject of numerous studies for the condensed-matter physics community [1–6]. This appears to be understandable from the point view of fundamental research since the superconductivity confined in a two-dimensional (2D) interface exhibits many exotic phenomena that have certain counterparts in layered cuprates and iron-based superconductors [6–8], and thus providing with unprecedented opportunities to crack the mystery of high-temperature (T_c) superconductivity. It seems more significant insofar as the superconducting technology application is concerned. By constructing and tailoring heterostructures, the interfaces might benefit from two building blocks and exhibit unexpectedly high T_c [1,9]. Moreover, the modified fluctuations, electron correlations, and spin-orbit coupling in reduced dimensionality are potential factors to drive the emergence of novel quantum phenomena [4,10], paving the unique way to pursue more promising technologies. Despite extensive research efforts, however, a unified microscopic picture on how the interface superconductivity is prompted remains as enigmatic as ever [11–13], in part due to the complexity of interface involved. It is thus highly tempting to build much simpler superconducting heterostructures.

Tin diselenide ($SnSe_2$), a main-group metal dichalcogenide and being superconducting by organometallic intercalation [14–17], exhibits a similar layered structure to that of graphene and transition-metal dichalcogenides. Recent extensive studies have revealed rich physics and potential applications in these materials [18]. For example, superconducting and electrically gated metal dichalcogenides not only show many properties analogous to those observed in cuprates [19], but also present new electron pairing with nontrivial topology, such as 2D Ising superconductivity protected by spin-valley locking [20–22]. In this study, we grow high-quality $SnSe_2$ films on graphitized SiC(0001) substrate, and demonstrate the superconductivity at the interface of $SnSe_2$ and graphene by using scanning tunneling microscopy (STM). By exploring the variances of film thickness and graphene, we tailor the heterostructures and reveal a two-dimensional electron gas (2DEG) formed at the interface, which bears the responsibility for superconductivity observed there.

Our experiments are carried out on an ultrahigh vacuum cryogenic STM system (Unisoku) equipped with a molecular beam epitaxy (MBE) for sample preparation. The base pressure of both chambers is better than 1.0×10^{-10} Torr. Nitrogen-doped SiC(0001) wafers (0.1 Ω cm) are graphitized by being heated to 1350 °C, resulting in a bilayer graphene-dominant surface [23]. High-purity Sn (99.9999%) and Se (99.999%) sources are coevaporated from standard effusion cells on the graphitized SiC(0001) substrate at ∼210 °C, giving rise to a layer-by-layer epitaxial growth of $SnSe_2$ films. During the MBE growth, a Se-rich atmosphere is adopted to compensate for the loss of volatile Se molecules, bearing a similar growth dynamics to that for other metal selenides [24]. Once the growth is finished, the samples are *in situ* transferred into the STM head for data collection. A polycrystalline PtIr tip, cleaned by electron beam heating and calibrated on epitaxial Ag/Si(111) films, is used throughout the experiments. Tunneling spectra and maps are measured at 0.4 K by using a standard lock-in technique with a small bias modulation of 0.1 meV at 931 Hz, unless otherwise specified.

As a layered semiconductor, $SnSe_2$ crystallizes into the CdI_2-type structure and consists of a hexagonally packed layer of Sn atoms sandwiched between two layers of Se anions [22,25]. The intralayer Sn-Se bonds are predominantly covalent in nature, whereas the forces between the sandwich layers are of weak van der Waals (vdWs) type. Figure 1(a) schematically draws the geometry of epitaxial $SnSe_2$ films on graphitized SiC(0001) substrate, in which the middle bilayer graphene and the top $SnSe_2$ films are of weak vdWs

*clsong07@mail.tsinghua.edu.cn
†xucunma@mail.tsinghua.edu.cn
‡qkxue@mail.tsinghua.edu.cn

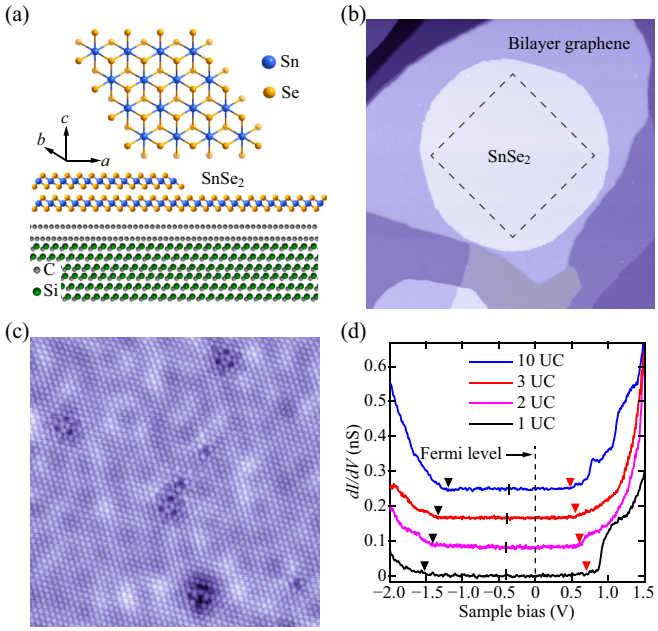

FIG. 1. (a) Sketch of a $SnSe_2$/graphene heterostructure. (b) Topographic image (300 nm × 300 nm, $V = 3.5$ V, $I = 20$ pA) of *in situ* grown $SnSe_2$ films on graphitized SiC(0001). The dashed square marks the region where ZBC maps are acquired. (c) Zoom-in STM topography (18 nm × 18 nm, $V = 50$ mV, $I = 100$ pA) on 1-UC $SnSe_2$ film. The bright spots denote the Se atoms at the top layer. (d) Thickness-dependent dI/dV spectra of $SnSe_2$ films. The black and red triangles mark VBM and CBM near the Γ point of $SnSe_2$, respectively, with their middles marked by short vertical lines. Tunneling gap is set at $V = 1.5$ V and $I = 150$ pA. The lock-in bias modulation has a magnitude of 10 meV.

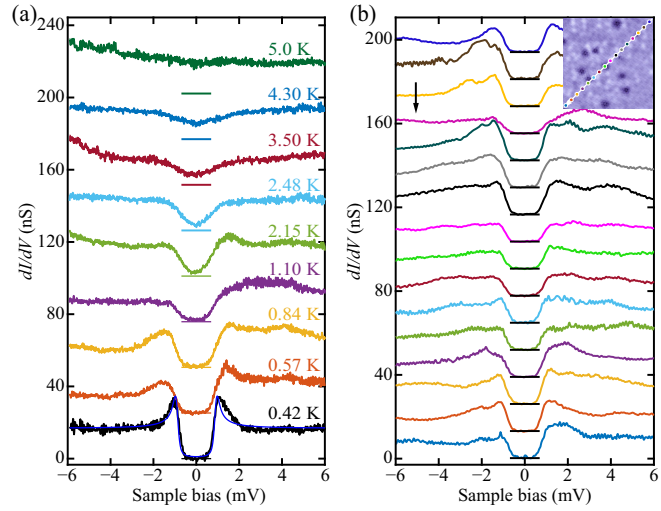

FIG. 2. (a) Tunneling dI/dV spectra ($V = 6$ mV, $I = 100$ pA) of 1-UC $SnSe_2$ film on bilayer graphene as a function of temperature as indicated. For clarity the spectra have been vertically offset, with their zero conductance positions marked by correspondingly colored horizontal lines. The same convention is used throughout, unless otherwise noted. The blue line at the bottom shows the best fit of experimental data (black curve) to the BCS Dynes formula with a single isotropic *s*-wave gap. (b) A series of dI/dV spectra ($V = 10$ mV, $I = 100$ pA) acquired at 0.4 K and along a 40 nm trajectory in the inserted STM image (30 nm × 30 nm, $V = 10$ mV, $I = 100$ pA). Instead of colored lines, the black lines mark the zero conductance positions for clarity.

interactions. Figure 1(b) typifies a constant-current STM topography of as-grown $SnSe_2$ films, with a nominal thickness of ∼0.7 unit cell (UC; one Se-Sn-Se triple layer). A magnified STM image reveals the top Se atoms, which are in a hexagonal close packing and spaced $\sim 3.82 \pm 0.03$Å apart [Fig. 1(c)]. This value, together with the extracted out-of-plane lattice constant of approximately 6.1 Å by measuring the height difference across the steps of $SnSe_2$ films, matches excellently with the lattice parameters of $SnSe_2$ [25].

We carry out the film-thickness-dependent measurements and find no observable variation in the lattice constants. However, the electronic band structures vary significantly with film thickness, as clearly revealed in Fig. 1(d). As the film thickness reduces, both the valance and conduction bands of $SnSe_2$ films move away from the Fermi level (E_F), leading to an obvious increase in the band gap. This is explained in the Supplemental Material [26], in which we quantitatively measure the energy positions of valance band maximum (VBM) and conduction band minimum (CBM) of $SnSe_2$ as well as the band gaps (Supplemental Material Fig. S1). The increased band gaps are attributed to the poor electrostatic screening and enhanced quantum confinement of electrons in few-layer $SnSe_2$ systems [27]. Despite these variations, the middle point between VBM and CBM changes little with the film thickness and is pinned at ∼0.4 eV below E_F.

Strikingly, in the large semiconducting band gap high-resolution tunneling spectroscopy within a narrower energy window of ±6 meV, as represented by the black curve in Fig. 2(a), discloses an E_F-symmetric and fully gapped density of states (DOS). We consider its origin from superconductivity. In some regions (∼25%), the superconducting energy gap has pronounced coherence peaks and can be reasonably described by the well-known BCS Dynes expression with a single isotropic *s*-wave gap and adjustable lifetime broadening [28]. A representative fit to such a spectrum in Fig. 2(a) yields an energy gap with magnitude $\Delta = 0.95$ meV (blue line). The temperature dependence of the tunneling spectra reveals the progressive suppression of superconducting coherence peaks and lifting of zero-bias conductance (ZBC) at elevated temperatures [Fig. 2(a)]. At last, the superconducting gap completely vanishes at temperatures close to a transition temperature T_c of 4.84 K [Fig. S2(a)].

It is worth noting that the superconducting gap critically depends on the STM tip position on the $SnSe_2$ films and exhibits significant spatial inhomogeneity [Fig. 2(b)], which might originate from the structural ripples of epitaxial graphene related to the $6\sqrt{3} \times 6\sqrt{3}$ reconstruction on SiC(0001) [23]. This is evident from the STM image in Fig. 1(c), where the underlying superstructure can be clearly seen and might serve as disorder to suppress the coherence peaks [29–31]. Albeit with site-dependent fine structure, we notice that there always exists a vanishing DOS over a finite energy range near E_F for all the dI/dV spectra. This suggests a rather conventional character of the superconductivity with

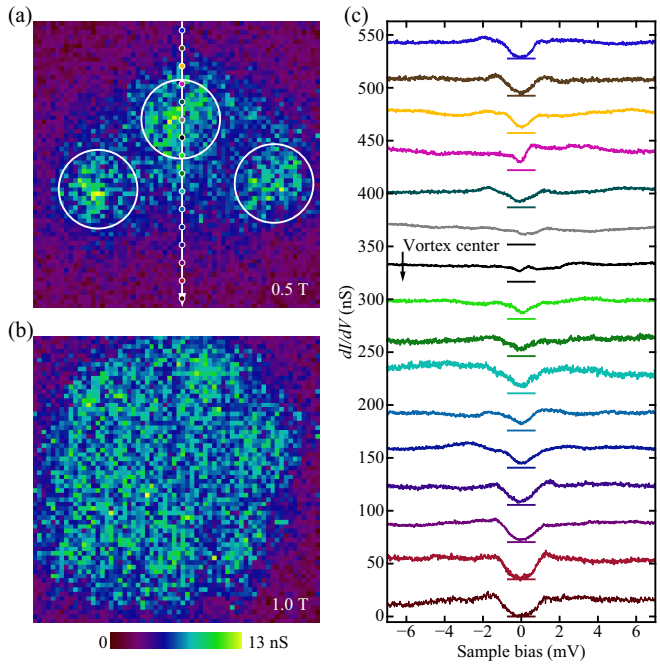

FIG. 3. (a) ZBC map (120 nm × 120 nm) showing three individual isolated vortices (emphasized by white circles) of a 1-UC $SnSe_2$/graphene heterostructure at 0.5 T. The colored dots along the arrowed line mark the positions where the dI/dV spectra of the same color code are acquired in (c). The tunneling junction [also applies to (b) and (c)] is set at $V = 8$ mV and $I = 100$ pA. (b) ZBC map at a higher magnetic field of 1.0 T. (c) Linecut of dI/dV spectra across a vortex core in (a) and at 0.4 K.

a fully gapped order parameter that is more likely phonon mediated. A statistical study of gap magnitude Δ [Fig. S2(b)], defined as half the energy separation between the two gap edges, reveals a predominant distribution of Δ of 1.05 meV. This somewhat overestimates the Δ and results in an upper limit of the reduced gap ratio $2\Delta/k_BT_c \sim 5.04$. The superconductivity in $SnSe_2$/graphene is of strong-coupling type.

To further confirm the superconductivity, we map out the spatial-resolved ZBC (64 pixels × 64 pixels) on a 120 nm × 120 nm field of view of $SnSe_2$ films at various magnetic fields, as drawn in Figs. 3(a) and 3(b). Distinct from the zero-field featureless ZBC map [Fig. S3(a)], here the yellow regions with elevated ZBC [Fig. S3(b)] signify the penetration of vortices into the heterostructure. Three vortices are expected and actually identified at 0.5 T [Fig. 3(a)]. The superconducting coherence length ξ is estimated to be $\sim 17.2 \pm 0.3$ nm [Fig. S3(c)], giving rise to a critical field $H_{c2} \sim 1.1$ T via $H_{c2} = \Phi_0/2\pi\xi^2$. At a higher field of 1.0 T near H_{c2}, the vortices get close to each other and are not individually discernible [Fig. 3(b)]. The irregular vortex core might be due to the inhomogeneous superconductivity in a $SnSe_2$/graphene heterostructure [Fig. 2(b)], bearing a striking resemblance to cuprate superconductors with the notorious electronic inhomogeneity [32]. Plotted in Fig. 3(c) are a series of dI/dV spectra taken at equal separations (7.5 nm) across a vortex core in Fig. 3(a). Evidently, the spatial dependence of the tunneling conductance spectra reveals the disappearance of the superconducting gap at sites close to the vortex center (black curve). No quasiparticle bound state is found within the vortex core [Fig. S3(b)], primarily due to the graphene ripple-induced electron scattering [33], which reduces the electron mean free path and pushes the superconducting $SnSe_2$/graphene into the dirty limit [34]. Our direct visualization of vortices provides unambiguous evidence of superconductivity in $SnSe_2$/graphene heterostructures.

In what follows, we engineer the heterostructure by exploring the variances of graphene substrate and $SnSe_2$ film thickness, and shed light on the mechanism of superconductivity. Enumerated in Fig. 4(a) are the two key results we disclose. First, the superconducting gap reduces in magnitude Δ and gets filled with subgap DOS as the $SnSe_2$ film thickness is increased [cf. the three curves in the middle of Fig. 4(a)]. This indicates the suppressed superconductivity with increasing $SnSe_2$ thickness, and provides the first piece of evidence that the superconductivity occurs at the interface of $SnSe_2$ and graphene. Indeed, the tunneling spectrum on thicker films reveals a semiconducting character and the STM tip can never be stabilized at bias voltages smaller than 0.1 V. Second, the number of graphene layers plays a vital role in the superconducting state. Although the bilayer and trilayer graphene give rise to a U-shaped pairing gap, the heterostructures composed of $SnSe_2$ and monolayer graphene are typically sized of V-shaped gaps with nonzero subgap DOS at E_F and no coherence peak (green curve). To reveal that this does not happen by accident, we map out the zero-field spatial ZBC of $SnSe_2$ grown on a substrate region of coexisting monolayer, bilayer, and trilayer graphene [Fig. 4(b)]. As confirmed in Fig. 4(c), the $SnSe_2$ films situated on monolayer graphene universally exhibit enhanced ZBC and weak superconductivity. This is consistent with the preferential vortex pinning at locations of the $SnSe_2$/monolayer graphene heterostructure (Fig. S4).

In the $SnSe_2$/graphene heterostructures, a simple explanation of the observed superconductivity by either strain effects or element interdiffusion seems unlikely. For vdWs epitaxy, strains are often small, and if they came into play the superconductivity should not rely significantly on the number of graphene layers as observed in Fig. 4(a). Moreover, we reveal no signature of superconductivity on uncovered graphene after the $SnSe_2$ growth (Fig. S5), which rules out a possible cause of superconductivity by diffusion of Sn and/or Se into graphene. On the other hand, an inverse diffusion of carbon into $SnSe_2$ films is nearly impossible as well at the lower growth temperature of 210 °C. Given that the superconductivity is sharply dependent on the two materials building the heterostructure [Fig. 4(a)], a more plausible explanation would seem to be that the superconductivity stems from the interface between $SnSe_2$ and graphene. Learning that epitaxial graphene on SiC has a lower work function (4.2–4.4 eV) [35] than $SnSe_2$ (~5.3 eV) [36], upon contact electrons would flow from graphene to $SnSe_2$, leading to a downward band bending of the $SnSe_2$ bands and electron accumulation near the interface. At equilibrium, their Fermi levels are aligned and a 2DEG is created at the $SnSe_2$/graphene interface. This is illustrated in the inserted energy band diagram of Fig. 4(d), and supported by our experiments. Shown in Fig. 4(d) are the thickness-dependent dI/dV spectra recorded in an intermediate energy range of ±0.5 eV, from which two findings are immediately revealed. First, each dI/dV spectrum presents

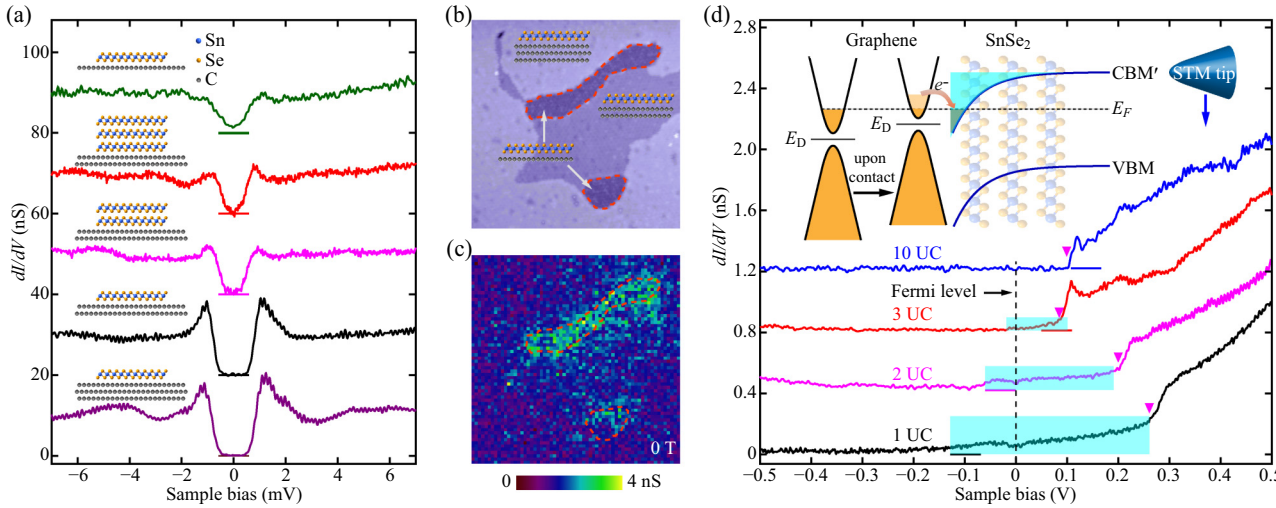

FIG. 4. (a) Tunneling spectra at 0.4 K vs sketched $SnSe_2$/graphene heterostructures on every upper-left corner of the curves. For simplicity the atoms of SiC are not displayed. The tunneling junction is set at $V = 10$ mV and $I = 100$ pA except for the bottom one ($V = 8$ mV, $I = 100$ pA). (b) A 98 nm × 98 nm STM topographic image ($V = 10$ mV, $I = 100$ pA) of 1-UC $SnSe_2$ films prepared on monolayer, bilayer, and trilayer grpaphene coexisting substrate. The red dashes encircle the region of $SnSe_2$ films situated on monolayer graphene. (c) Simultaneous ZBC map (64 pixels × 64 pixels) revealing graphene layer-dependent conductance contrast at zero field. (d) Dependence of dI/dV spectra ($V = 0.5$ V, $I = 150$ pA) on the $SnSe_2$ film thickness, measured in an intermediate energy range of ±0.5 eV. The lock-in has a bias modulation of 5 meV. The magenta triangles mark the CBM at the M point of $SnSe_2$, located far above E_F (vertical dashes). Inset shows the energy band scheme for a $SnSe_2$/graphene heterostructure. Electron transfer from graphene to the $SnSe_2$ films is indicated by the orange arrow. The band gap opening near the Dirac point (E_D) of graphene due to the SiC substrate is also shown.

a prominent drop of DOS around 0.1–0.3 eV, which we interpret as DOS variation from the conduction band at the M high-symmetry point of the Brillouin zone in $SnSe_2$ [26,27]. This allows for determination of its minimum (dubbed as CBM′) and indirect band gap E_g^{in} of $SnSe_2$ (Fig. S1), which shows a quantitative agreement with the theoretical calculations [27]. Second, and the most significantly, the band edges get rounded and show an increasingly long nonzero DOS tail (cyan-marked) toward E_F with reduced film thickness. A closer inspection of the band scheme in Fig. 4(d) reveals immediately its origin from the 2DEG confined at the $SnSe_2$/graphene interface. Note that all bulk bands of $SnSe_2$ are positioned far away from E_F (e.g., >0.2 eV for 1-UC $SnSe_2$) and the nonzero DOS in thin films originate solely from 2DEG; we argue that the superconductivity occurs due to the formation of 2DEG in a $SnSe_2$/graphene heterostructure. Indeed, the nonzero DOS and 2DEGs get shrinking with the film thickness, matching well with the suppressed superconductivity in thick $SnSe_2$ films.

Finally, the graphene layer-dependent superconductivity seems counterintuitive since monolayer graphene has the smallest work function [35] and is more beneficial to the 2DEG formation and superconductivity. However, one should also be aware that monolayer graphene has larger structural ripples and is more disordered relative to bilayer graphene [23]. They might cause strong electron scattering and then suppress the superconductivity. Besides, a more relevant factor may be the relatively lower carrier density in monolayer graphene as compared to bilayer and trilayer graphene [37]. This leads to a 2DEG with low concentration, which, in conjunction with the strong scattering, might be responsible for the V-shaped gap structure and suppressed superconductivity. A recent study of a $SnSe_2$ bilayer on graphite with much lower carrier density [38] revealed V-shaped spectral gaps as well, but with an unreasonably large gap size Δ of ∼16–22 meV as compared to T_c, which were interpreted as a signature of unconventional superconductivity [39]. However, without vortex imaging and the careful interface engineering explored here, whether the large gap relates to superconductivity is questionable.

Our detailed STM scrutiny of $SnSe_2$ films on graphene has discovered clear interface superconductivity with a rather conventional character. The revealed mechanism of superconductivity due to the formation of 2DEG might shed important insight into interface superconductivity as well as the mechanism of high-T_c superconductivity in compounds made of heterostructures at the atomic plane limit. Moreover, our study suggests that the semiconducting $SnSe_2$ and its heterostructures can serve as ideal platforms to explore the novel physics of interface superconductivity. Further interface engineering through preparing $SnSe_2$ on substrates with high carrier densities and strong electron-phonon coupling (e.g., perovskite oxide $SrTiO_3$) might promote superconductivity with a higher critical temperature.

This work is financially supported by the Ministry of Science and Technology of China (Grants No. 2017YFA0304600, No. 2015CB921001, and No. 2016YFA0301004), the National Natural Science Foundation of China (Grants No. 11427903, No. 11504196, No. 11634007, and No. 11774192), and in part by the Beijing Advanced Innovation Center for Future Chip (ICFC). C.L.S. acknowledges support from the National Thousand-Young-Talents Program and Tsinghua University Initiative Scientific Research Program.

[1] Q. Y. Wang, Z. Li, W. H. Zhang, Z. C. Zhang, J. S. Zhang, W. Li, H. Ding, Y. B. Ou, P. Deng, K. Chang, J. Wen, C. L. Song, K. He, J. F. Jia, S. H. Ji, Y. Y. Wang, L. L. Wang, X. Chen, X. C. Ma, and Q. K. Xue, Chin. Phys. Lett. **29**, 037402 (2012).

[2] N. Reyren, S. Thiel, A. D. Caviglia, L. F. Kourkoutis, G. Hammerl, C. Richter, C. W. Schneider, T. Kopp, A.-S. Rüetschi, D. Jaccard, M. Gabay, D. A. Muller, J. M. Triscone, and J. Mannhart, Science **317**, 1196 (2007).

[3] A. Gozar, G. Logvenov, L. F. Kourkoutis, A. T. Bollinger, L. A. Giannuzzi, D. A. Muller, and I. Božović, Nature (London) **455**, 782 (2008).

[4] Q. L. He, H. C. Liu, M. Q. He, Y. H. Lai, H. T. He, G. Wang, K. T. Law, R. Lortz, J. N. Wang, and I. K. Sou, Nat. Commun. **5**, 4247 (2014).

[5] Y. Zhong, Y. Wang, S. Han, Y. F. Lv, W. L. Wang, D. Zhang, H. Ding, Y. M. Zhang, L. Wang, K. He, R. D. Zhong, J. A. Schneeloch, G. D. Gu, C. L. Song, X. C. Ma, and Q. K. Xue, Sci. Bull. **61**, 1239 (2016).

[6] Y. Saito, T. Nojima, and Y. Iwasa, Nat. Rev. Mater. **2**, 16094 (2017).

[7] C. Richter, H. Boschker, W. Dietsche, E. Fillis-Tsirakis, R. Jany, F. Loder, L. F. Kourkoutis, D. A. Muller, J. R. Kirtley, C. W. Schneider, and J. Mannhart, Nature (London) **502**, 528 (2013).

[8] Y. Saito, Y. Kasahara, J. Ye, Y. Iwasa, and T. Nojima, Science **350**, 409 (2015).

[9] J. F. Ge, Z. L. Liu, C. Liu, C. L. Gao, D. Qian, Q. K. Xue, Y. Liu, and J. F. Jia, Nat. Mater. **14**, 285 (2015).

[10] X. Gong, M. Kargarian, A. Stern, D. Yue, H. Zhou, X. Jin, V. M. Galitski, V. M. Yakovenko, and J. Xia, Sci. Adv. **3**, e1602579 (2017).

[11] J. Wu, O. Pelleg, G. Logvenov, A. T. Bollinger, Y. J. Sun, G. S. Boebinger, M. Vanević, Z. Radović, and I. Božović, Nat. Mater. **12**, 877 (2013).

[12] D. Huang and J. E. Hoffman, Annu. Rev. Condens. Matter Phys. **8**, 311 (2017).

[13] C. Brun, T. Cren, and D. Roditchev, Super. Sci. Tech. **30**, 013003 (2016).

[14] C. A. Formstone, E. T. FitzGerald, D. O'Hare, P. A. Cox, M. Kurmoo, J. W. Hodby, D. Lillicrap, and M. Goss-Custard, J. Chem. Soc., Chem. Commun. **0**, 501 (1990).

[15] C. A. Formstone, M. Kurmoo, E. T. FitzGerald, P. A. Cox, and D. O'Hare, J. Mater. Chem. **1**, 51 (1991).

[16] D. O'Hare, H. V. Wong, S. Hazell, and J. W. Hodby, Adv. Mater. **4**, 658 (1992).

[17] Z. J. Li, Y. C. Zhao, K. Mu, H. Shan, Y. Q. Guo, J. J. Wu, Y. Q. Su, Q. R. Wu, Z. Sun, A. D. Zhao, X. F. Cui, C. Z. Wu, and X. Y, J. Am. Chem. Soc. **139**, 16398 (2017).

[18] G. R. Bhimanapati, Z. Lin, V. Meunier, Y. Jung, J. Cha, S. Das, D. Xiao, Y. Son, M. S. Strano, V. R. Cooper, L. B. Liang, S. G. Louie, E. Ringe, W. Zhou, S. S. Kim, R. R. Naik, B. G. Sumpter, H. Terrones, F. N. Xia, Y. L. Wang, J. Zhu, D. Akinwande, N. Alem, J. A. Schuller, R. E. Schaak, M. Terrones, and J. A. Robinson, ACS Nano **9**, 11509 (2015).

[19] R. A. Klemm, Physica C **514**, 86 (2015).

[20] J. M. Lu, O. Zheliuk, I. Leermakers, N. F. Q. Yuan, U. Zeitler, K. T. Law, and J. T. Ye, Science **350**, 1353 (2015).

[21] Y. Saito, Y. Nakamura, M. S. Bahramy, Y. Kohama, J. Ye, Y. Kasahara, Y. Nakagawa, M. Onga, M. Tokunaga, T. Nojima, Y. Yanase, and Y. Iwasa, Nat. Phys. **12**, 144 (2016).

[22] J. W. Zeng, E. F. Liu, Y. J. Fu, Z. Y. Chen, C. Pan, C. Y. Wang, M. Wang, Y. J. Wang, K. Xu, S. H. Cai, X. X. Yan, Y. Wang, X. W. Liu, P. Wang, S. J. Liang, Y. Cui, H. Y. Hwang, H. T. Yuan, and F. Miao, Nano Lett. **18**, 1410 (2018).

[23] J. Hass, W. A. De Heer, and E. H. Conrad, J. Phys.: Conden. Matter **20**, 323202 (2008).

[24] C. L. Song, Y. L. Wang, Y. P. Jiang, Z. Li, L. Wang, K. He, X. Chen, X. C. Ma, and Q. K. Xue, Phys. Rev. B **84**, 020503 (2011).

[25] C. Y. Fong and M. L. Cohen, Phys. Rev. B **5**, 3095 (1972).

[26] See Supplemental Material at http://link.aps.org/supplemental/10.1103/PhysRevB.98.220508 for details on semiconducting band gaps, superconductivity, and vortex pinning.

[27] J. M. Gonzalez and I. I. Oleynik, Phys. Rev. B **94**, 125443 (2016).

[28] R. C. Dynes, V. Narayanamurti, and J. P. Garno, Phys. Rev. Lett. **41**, 1509 (1978).

[29] M. Mondal, A. Kamlapure, M. Chand, G. Saraswat, S. Kumar, J. Jesudasan, L. Benfatto, V. Tripathi, and P. Raychaudhuri, Phys. Rev. Lett. **106**, 047001 (2011).

[30] Y. Noat, V. Cherkez, C. Brun, T. Cren, C. Carbillet, F. Debontridder, K. Ilin, M. Siegel, A. Semenov, H.-W. Hübers, and D. Roditchev, Phys. Rev. B **88**, 014503 (2013).

[31] C. Brun, T. Cren, V. Cherkez, F. Debontridder, S. Pons, D. Fokin, M. C. Tringides, S. Bozhko, L. B. Ioffe, B. L. Altshuler, and D. Roditchev, Nat. Phys. **10**, 444 (2014).

[32] Ø. Fischer, M. Kugler, I. Maggio-Aprile, C. Berthod, and C. Renner, Rev. Mod. Phys. **79**, 353 (2007).

[33] M. I. Katsnelson and A. K. Geim, Philos. Trans. A: Math. Phys. Eng. Sci. **366**, 195 (2008).

[34] Ch. Renner, A. D. Kent, P. Niedermann, Ø. Fischer, and F. Lévy, Phys. Rev. Lett. **67**, 1650 (1991).

[35] S. Mammadov, J. Ristein, J. Krone, C. Raidel, M. Wanke, V. Wiesmann, F. Speck, and T. Seyller, 2D Mater. **4**, 015043 (2017).

[36] T. Shimada, F. S. Ohuchi, and B. A. Parkinson, Jpn. J. Appl. Phys. **33**, 2696 (1994).

[37] T. Ohta, A. Bostwick, J. L. McChesney, T. Seyller, K. Horn, and E. Rotenberg, Phys. Rev. Lett. **98**, 206802 (2007).

[38] C. A. Klein and W. D. Straub, Phys. Rev. **123**, 1581 (1961).

[39] Y. H. Mao, H. Shan, J. R. Wu, Z. J. Li, C. Z. Wu, X. F. Zhai, A. D. Zhao, and B. Wang, arXiv:1712.10100.